

# Directing Sequential Self-Organization with Self-Assembled Nanocrystals

Published as part of *Crystal Growth & Design* special issue “Celebrating Mike Ward’s Contributions to Molecular Crystal Growth”.

Ariane V. Mader, René M. Williams, Joanna Aizenberg,\* and Willem L. Noorduin\*



Cite This: <https://doi.org/10.1021/acs.cgd.4c01450>



Read Online

ACCESS |



Metrics & More

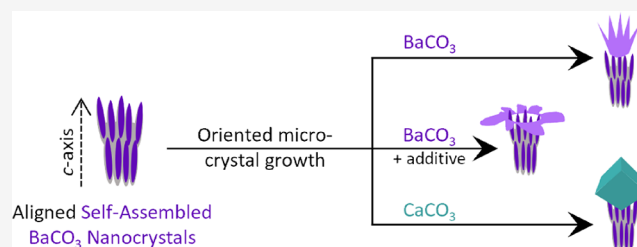


Article Recommendations



Supporting Information

**ABSTRACT:** Sequential self-organization can be used to design the hierarchy and complexity of materials beyond what is possible with single-step synthesis. However, such sequential approaches introduce additional challenges in maintaining control over the process. To guide the position and orientation of newly nucleated material, we propose the use of self-assembled nanocrystals (SANCs). We test the potential of SANCs in  $\text{BaCO}_3/\text{SiO}_2$  nanocomposites, also termed silica biomorphs, to direct the formation of nascent microscopic crystals. We find that SANCs can direct the location and crystallographic orientation of microcrystals at the nucleation stage, while the material, polymorph, and growth behavior of the crystal can be tuned largely independently. Using ion exchange reactions, we show that structures can be unified into a single material of interest in subsequent steps. This level of control over material position, orientation, and chemical composition allows for the retrosynthetic design of complex hierarchical structures.



## INTRODUCTION

Self-organization can form intricate materials, with structures exhibiting high levels of hierarchy and complexity. These complex architectures can translate into exceptional material properties for functional applications in fields such as electronics, catalysis, and optics.<sup>1–8</sup> To further enhance the structural and functional complexity achievable with single-step self-organization approaches, these processes can be carried out in a sequential manner.<sup>9,10</sup> However, guiding the organization of a material through multiple steps presents new challenges in maintaining control over each step toward the final material composition and shape. In addition to controlling shape and composition of the newly generated material, it is often desirable to direct the specific location and orientation of attachment to the previously formed architecture. Therefore, it is crucial to develop strategies for spatial and orientational control in order to realize the potential of sequential self-organization for generating new and increasingly complex advanced functional materials.

Different strategies have already been developed to guide the location and orientation of crystal nucleation. Preferred nucleation sites can be achieved using methods such as seeding, surface templating, or chemical functionalization.<sup>11–19</sup> A widely used chemical functionalization of surfaces consists of self-assembled monolayers (SAMs), in which molecules are adsorbed to a surface, usually in a tightly packed and well-ordered arrangement.<sup>20,21</sup> The chemistry, orientation, and

spatial distribution of the SAM's functional groups can be used to control the nucleation of crystals on top of the SAM and also stabilize specific crystal facets and crystal polymorphs.<sup>11,18,19</sup> Nature has developed various strategies to precisely align anisotropic biomineral crystals for optimal function. For instance, some organisms use birefringent forms<sup>22</sup> of the biomineral calcium carbonate for optical applications,<sup>23,24</sup> highlighting the crucial importance of specific crystallographic orientation for correct function. Although it is oftentimes unclear which strategies organisms use for this precise alignment, many organisms form aligned nanocrystals, which enhance the material properties and can be crucial for the organism's survival.<sup>5,6,25–28</sup> This prompted us to consider the use of artificial self-assembled nanocrystals (SANCs) analogous to SAMs to direct crystal nucleation (Figure 1A).

A suitable system to explore the functionality of SANCs in guiding sequential self-organization is the class of nanocomposites known as biomorphs, a term initially coined due to their resemblance to natural forms.<sup>29,30</sup> These nanocomposites are present in a variety of curved unafaceted microshapes,

**Received:** October 21, 2024

**Revised:** November 24, 2024

**Accepted:** November 25, 2024

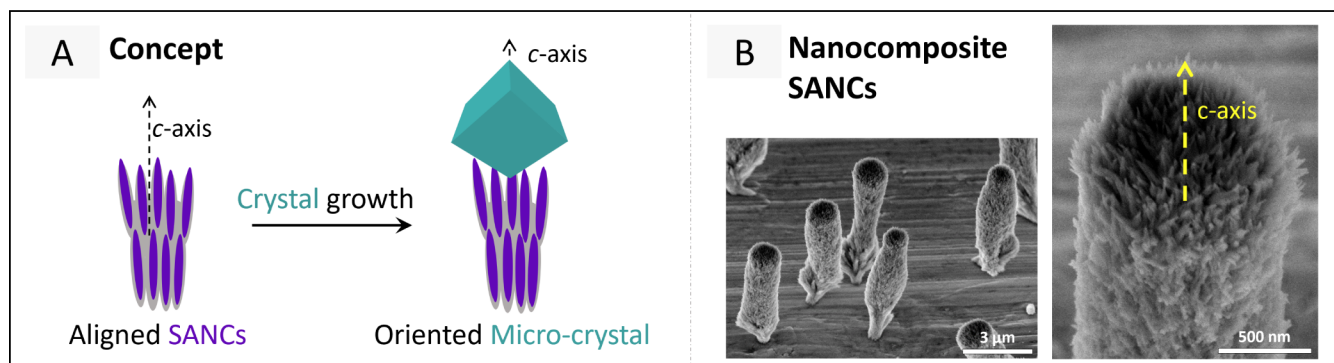


**Figure 1.** A) Concept drawing to illustrate how self-assembled nanocrystals (SANCs) can direct the growth of nascent microcrystals. B)  $\text{BaCO}_3/\text{SiO}_2$  nanocomposite structures with stem shapes, illustrating the coalignment of their constituent SANCs.

resembling stems, spirals, leaves, vases, and corals. The unique shapes arise from the coprecipitation of amorphous silica and a carbonate salt; for example, barium carbonate and amorphous silica can form barium carbonate/silica ( $\text{BaCO}_3/\text{SiO}_2$ ) nanocomposites.<sup>9</sup> This coprecipitation reaction can be influenced to generate selected nanocomposite shapes with functional properties.<sup>9,31</sup> Morphological control can be achieved by tuning bulk solution conditions like pH or ion concentrations,<sup>9</sup> by introducing additives,<sup>32,33</sup> or by locally directing the growth using light and photochemistry.<sup>10,34,35</sup> Furthermore, the  $\text{BaCO}_3/\text{SiO}_2$  nanocomposites are not only versatile in shape but can also be functionalized with surface modifications or the exchange of their nanocrystal composition for a plethora of different functional materials through ion exchange reactions.<sup>7,36–39</sup>

Nanocomposites of  $\text{BaCO}_3/\text{SiO}_2$  are especially promising for sequential self-organization due to their internal organization. These microstructures consist of a collection of carbonate nanocrystals elongated along the *c*-axis direction and embedded in an amorphous silica matrix. The silica passivates the growth of the nanocrystals, such that only the tips at the growth front remain uncovered.<sup>9</sup> Therefore, the SANCs remain active only at very specific locations, thereby offering the opportunity to spatially direct the attachment of a new material.

The exposed nanocrystals at the growth front of  $\text{BaCO}_3/\text{SiO}_2$  nanocomposites have already been used as nucleation sites for other nanocomposite structures<sup>10</sup> and mesocrystals,<sup>40</sup> but not yet to crystallographically orient single crystals. It is known that microscopic crystals can guide the orientation of smaller crystals.<sup>14,41</sup> Conversely, structures as small as SAMs can dictate the orientation of larger crystals nucleating on them.<sup>11,18</sup> This leads us to wonder whether nanocrystals can similarly control the orientation of larger crystals. For this, the nanocrystals need to be sufficiently aligned, and in the case of the  $\text{BaCO}_3$  SANCs, their *c*-axis is aligned toward the growth front of the nanocomposites with a  $\sim 30^\circ$  spread (Figure 1B).<sup>38</sup> Despite this spread, it has been shown that the SANC alignment of the  $\text{BaCO}_3/\text{SiO}_2$  nanocomposites is sufficient to guide and directionally emit light.<sup>8</sup> This raises the question whether the SANCs of  $\text{BaCO}_3/\text{SiO}_2$  nanocomposites are able to orient the nucleation of microcrystals onto them.

In this study, we explore the potential of SANCs to direct sequential self-organization. We investigate this by using the SANCs in  $\text{BaCO}_3/\text{SiO}_2$  nanocomposites in combination with epitaxially matching microcrystals. We aim to control not only the material and crystal structure of the microcrystals but also

their position, crystallographic orientation, and shape with regard to the nanocomposites on which they nucleate. We show how SANCs can direct the position and orientation of microcrystal nucleation and envision other types of nucleation directors, thereby expanding the toolbox for sequential self-organization to create complex nanocomposites with tailored shapes and properties.

## RESULTS AND DISCUSSION

To test if we can use the SANCs to crystallographically orient nascent microcrystals, we grow different forms of  $\text{BaCO}_3$  crystals on top of  $\text{BaCO}_3/\text{SiO}_2$  nanocomposites. We select reaction conditions that favor the formation of nanocomposites with stem-like morphologies, as they exhibit *c*-axis alignment perpendicular to the substrate. This orientation facilitates the observation of active SANCs and their alignment at the former growth front. The primary challenge in the initial nanocomposite growth step lies in achieving selective silica passivation, ensuring that only the growth front remains uncoated. Prolonged growth could passivate the growth front, while a short growth time may result in insufficient silica precipitation on the rest of the structure. In both scenarios, spatial control for selective attachment during the next growth stage would be lost. The primary challenge in growing the microcrystal on the composite during the second step lies in tuning the reaction conditions for selective nucleation and growth at the exposed nanocrystals.

Following previously deployed procedures,<sup>9</sup> we first grow  $\text{BaCO}_3/\text{SiO}_2$  nanocomposites on a substrate immersed in an aqueous solution (20.2 mM  $\text{BaCl}_2$ , 8.65 mM  $\text{Na}_2\text{SiO}_3$ ) and then transfer the substrate to a second solution (20.2 mM  $\text{BaCl}_2$ , pH adjusted to 11 with 1 M  $\text{NaOH}$ ) to initiate the growth of microscopic  $\text{BaCO}_3$ . The  $\text{BaCO}_3$  formation in both steps is driven by the diffusion of  $\text{CO}_2$  from the air into the solution, which gradually increases the  $\text{BaCO}_3$  supersaturation. The resulting structures are visualized using scanning electron microscopy (SEM).

We observe that the new microscopic  $\text{BaCO}_3$  growth occurs exclusively at the top of the biomorph stems where the previous growth front was located, indicating precise spatial control over the new microscopic growth (Figure 2A,B). Moreover, the main growth direction along the *c*-axis of the microcrystals is oriented parallel to the *c*-axis of the SANCs, as can be seen by the continued elongated growth in the same direction as the nanocomposite. This suggests a sufficient SANC alignment to orient microcrystal nucleation and growth both spatially and crystallographically.

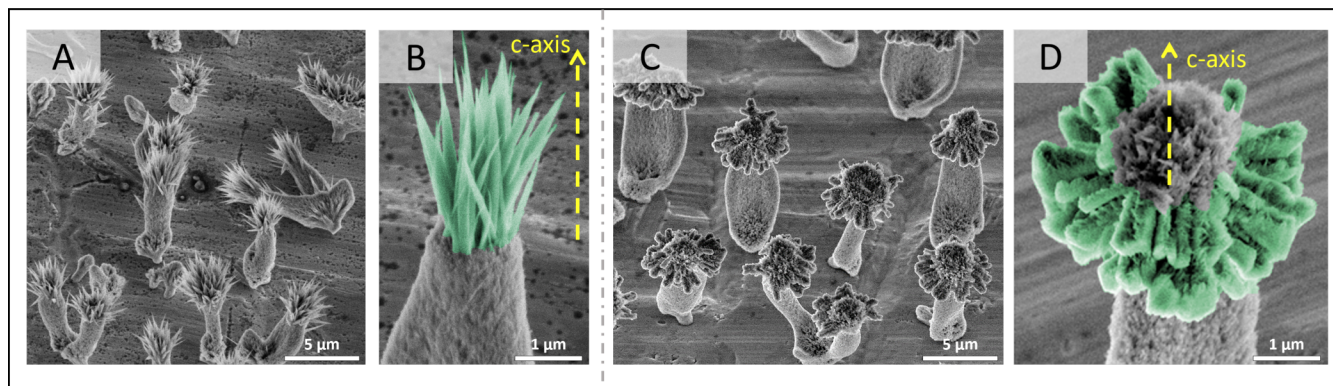


**Figure 2.** Crystallization of microscopic  $\text{BaCO}_3$  on SANCs in  $\text{BaCO}_3/\text{SiO}_2$  nanocomposites. A)  $\text{BaCO}_3/\text{SiO}_2$  nanocomposites with subsequent  $\text{BaCO}_3$  growth. B) Close-up of a structure grown under the same conditions as (A). C)  $\text{BaCO}_3/\text{SiO}_2$  nanocomposites with subsequent  $\text{BaCO}_3$  growth in the presence of an additive hampering the growth in the  $c$ -axis direction. D) Close-up of a structure grown under the same conditions as (C). The second growth phase in the close-up images (B) and (D) is false-colored in green to indicate the  $\text{BaCO}_3$  microcrystals.

Next, we tested whether we can grow a microscopic  $\text{BaCO}_3$  crystal extending perpendicularly to the SANC main growth. For this, we take advantage of the fixed orientation of the microcrystals when nucleating on the SANCs and focus on adjusting the growth behavior for the desired planar shape. It is known that the growth along the usual  $c$ -axis direction can be hindered by some additives, thereby promoting growth in the direction along the  $a/b$ -axes, which results in  $\text{BaCO}_3$  crystals with a planar appearance (Figure S2 in SI).<sup>42,43</sup> Inspired by this, we use a low concentration of silica as a growth-inhibiting additive (3.1 mM  $\text{Na}_2\text{SiO}_3$ , pH adjusted to 11 with 1 M NaOH) to create a  $\text{BaCO}_3$  crystal extending perpendicularly to the SANC growth direction.

The new growth of the  $\text{BaCO}_3$  microcrystals in the presence of a growth inhibitor still occurs at the previous growth front of the nanocomposites (Figure 2C,D). Additionally, as anticipated, the main growth direction of the microcrystal is along the  $a/b$ -axes parallel to the substrate instead of along the  $c$ -axis perpendicular to it. This makes the growth direction of the microscopic  $\text{BaCO}_3$  crystals also perpendicular to the main growth direction of the SANCs, giving the structure an overall T-shaped appearance. Even though the SANCs and the microcrystal consist of the same mineral and are oriented similarly with their crystallographic axes, their main growth proceeds in different directions. This shows that, while the SANCs direct the location and orientation of the microcrystal nucleation, the further growth of the microcrystal can be developed independently.

We explore whether we can also orient minerals of different chemical compositions on SANCs by taking advantage of epitaxial relationships. For this, we grow calcium carbonate ( $\text{CaCO}_3$ ) on the  $\text{BaCO}_3$  SANCs. An epitaxial relationship of  $\text{BaCO}_3$  to the  $\text{CaCO}_3$  polymorphs calcite and aragonite has already been reported, and these two  $\text{CaCO}_3$  polymorphs are able to align the  $c$ -axis of  $\text{BaCO}_3$  growing onto them.<sup>14</sup> We are wondering if the inverse is also possible, meaning whether  $\text{BaCO}_3$  SANCs can align  $\text{CaCO}_3$  microcrystals on top of them. To this aim, we grow  $\text{BaCO}_3/\text{SiO}_2$  nanocomposites with the previous reaction conditions and then reimmerse the substrate with nanocomposite structures into an aqueous solution containing a calcium ion source (typically 4.5 mM  $\text{CaCl}_2$ ). To grow  $\text{CaCO}_3$ , the solution can either be made basic by adding NaOH (1 M NaOH) or placed in a desiccator with ammonium carbonate salt.<sup>14,44</sup> The latter procedure ensures a

more gradual increase of  $\text{CaCO}_3$  supersaturation by gas diffusion, affecting both the  $\text{CO}_2$  saturation and the pH of the solution.

The  $\text{CaCO}_3$  composite structures display significantly different features depending on the supersaturation with which they were grown. The supersaturation can be influenced by many factors, including mineral ion concentration, pH, and nucleation site/SANC availability. In our experiments, we actively tune the supersaturation by varying the  $\text{CaCl}_2$  concentration and pH of the bulk solution, while the SANC availability depends on the growth density of the nanocomposites in the previous step. With a low  $\text{CaCO}_3$  supersaturation, we observe small calcite crystals grown across the nanocomposite structures (Figure 3A). This is likely caused by the dissolution of  $\text{BaCO}_3$ , releasing  $\text{CO}_3^{2-}$  into the solution, which then reprecipitates with the more supersaturated  $\text{Ca}^{2+}$  ions as  $\text{CaCO}_3$ . The calcite crystal distribution indicates no specific spatial preference, despite a presumably easier dissolution at the SANC growth front not yet coated by silica. With a high  $\text{CaCO}_3$  supersaturation, on the other hand, we find the kinetically preferred  $\text{CaCO}_3$  polymorph vaterite spread across the substrate (Figure 3C).<sup>45,46</sup> Vaterite does not have a preferential epitaxial relationship with  $\text{BaCO}_3$ <sup>14</sup> and is not found to grow on the  $\text{BaCO}_3/\text{SiO}_2$  nanocomposites. When the  $\text{CaCO}_3$  supersaturation is well-tuned between these two saturation extremes, we grow single crystals of rhombohedral calcite exclusively on top of the active SANCs (Figure 3B). The orientation of the calcite crystals is hard to determine and shows variation on each SANC, but they appear to be aligned with the  $c$ -axis of the SANC nanocrystals on which they are grown. These results demonstrate that it is indeed feasible to orient and direct the growth of a single microcrystal using SANCs of a different chemical composition.

The SANC organization in  $\text{BaCO}_3/\text{SiO}_2$  nanocomposites is largely independent of their collective microstructure shape. This suggests that it should also be possible to use the previously developed methods to grow microcrystals onto SANCs of differently shaped nanocomposites. To test this, we grow  $\text{BaCO}_3$  and  $\text{CaCO}_3$  microcrystals onto coral-shaped nanocomposites, respectively (Figure 4A), using the previously employed conditions. The growth front of the coral shape expands radially from its nucleus and offers a large surface for nucleation along the rim of the structure. Growing  $\text{BaCO}_3$  in the presence of growth inhibitor onto the coral-shaped

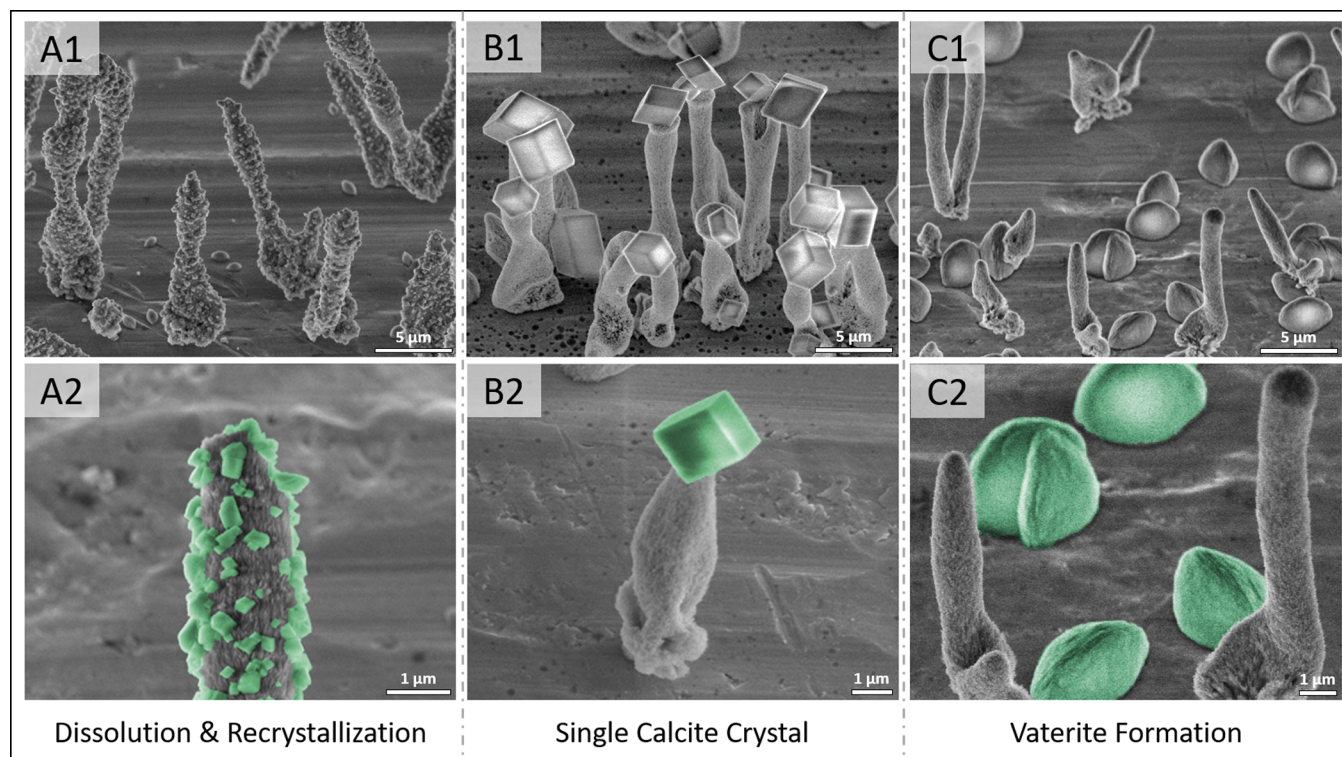


**Figure 3.** Crystallization of microscopic  $\text{CaCO}_3$  on SANCs in  $\text{BaCO}_3/\text{SiO}_2$  nanocomposites. A) Structures grown with low  $\text{CaCO}_3$  supersaturation, which led to dissolution and recrystallization. B) Structures grown with intermediate  $\text{CaCO}_3$  supersaturation, exhibiting single crystals grown on the SANCs. C) Structures grown with high  $\text{CaCO}_3$  supersaturation, leading to vaterite formation and no interaction with  $\text{BaCO}_3/\text{SiO}_2$  nanocomposites. The calcite growth is falsely colored in green in the close-up images (2).

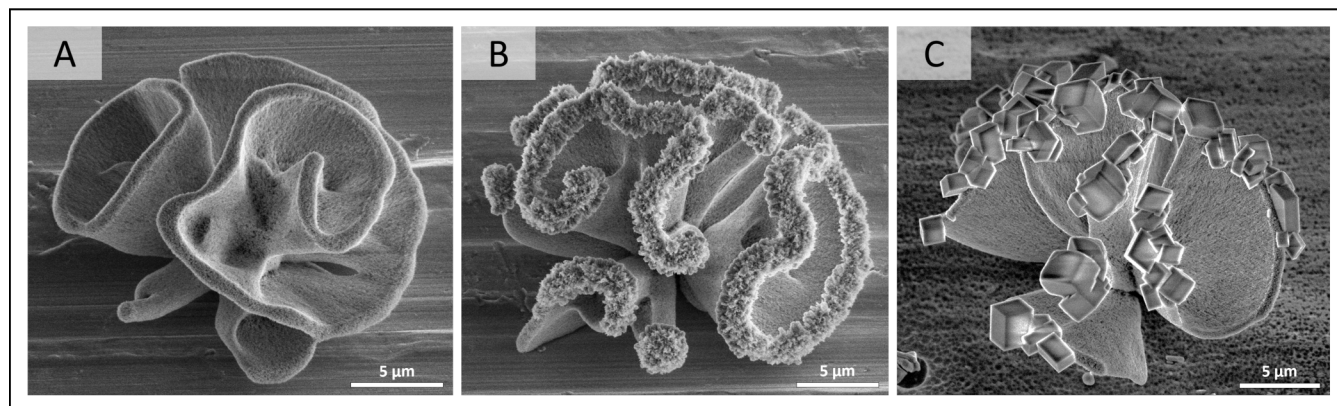


**Figure 4.** Crystallization of microscopic crystals on SANCs in coral-shaped  $\text{BaCO}_3/\text{SiO}_2$  nanocomposites. A) Coral-shaped  $\text{BaCO}_3/\text{SiO}_2$  nanocomposites. B) Coral-shaped  $\text{BaCO}_3/\text{SiO}_2$  nanocomposites with microscopic  $\text{BaCO}_3$  grown on top of it in the presence of  $\text{SiO}_2$  as a growth-modifying additive. C) Coral-shaped  $\text{BaCO}_3/\text{SiO}_2$  nanocomposites with microscopic  $\text{CaCO}_3$  grown on top of it.

nanocomposites results in a coral with what looks like a cocktail rim (Figure 4B). The new  $\text{BaCO}_3$  growth decorates and thickens the rim of the structure almost entirely, with the new growth perpendicular to the walls of the structure. Growing  $\text{CaCO}_3$  onto the coral shapes yields rhombohedral calcite crystals of varying sizes spread across the rim (Figure 4C). These results illustrate the versatility of the sequential self-organization approach, which is largely independent of the underlying shape of the SANC arrangement.

The sequential growth of mineral structures is not only interesting for the unique material combinations that can be created, but also for the new plethora of shapes that can be achieved. Shapes in itself can provide functional properties<sup>2</sup>

and can be accessed by combining common shapes of different materials. Similarly to retrosynthesis in organic chemistry, we can first determine a desired shape and then reengineer how and in which order the different building blocks of the structure can be constructed and merged without interfering with previous steps. Following this procedure, we can combine accessible, smaller building blocks to create more complex shapes using sequential self-organization. Due to the ion exchange methods already available,<sup>7,10,36–38</sup> structures consisting of different materials may later be converted into a single desired material.

Here, we show the potential of this concept by performing cation exchange toward  $\text{MnCO}_3$  on a structure made of a

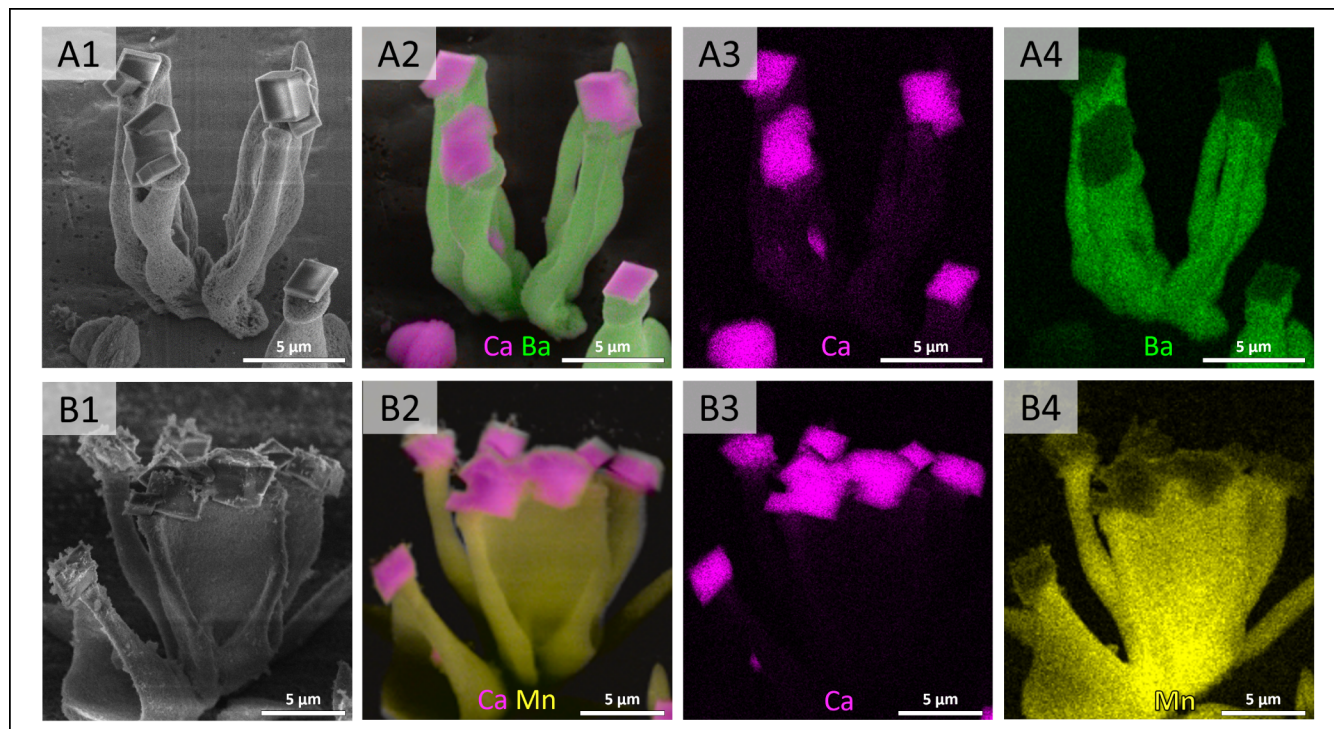


**Figure 5.** Conversion of  $\text{BaCO}_3/\text{SiO}_2$  nanocomposites with  $\text{CaCO}_3$  microcrystals toward  $\text{MnCO}_3$ . SEM images (1) are compared to energy-dispersive X-ray spectroscopy maps. Shown are map overlays (2) of a typical structure and individual element maps (3,4). A typical structure is shown before conversion (A) and after conversion (B). Pink indicates Ca, green Ba, and yellow Mn.

$\text{BaCO}_3/\text{SiO}_2$  nanocomposite and a  $\text{CaCO}_3$  microcrystal (Figure 5), following previously developed ion-exchange methods.<sup>10</sup> This is achieved by transferring the grown structures into an aqueous solution of  $\text{MnCl}_2$  (51.6 mM) under an argon atmosphere for 1 h, so the ion exchange reaction can take place. SEM with EDS (20 kV) shows that the very reactive nanocrystals of the composite are fully converted after this procedure (Figures S3 and S4 in SI). In contrast, the microcrystal still contains calcium ions, although at least the surface of the microcrystal also appears to contain manganese. There are several factors that could hinder the conversion of the microcrystals, including a much smaller surface-to-volume ratio, challenges in transporting the material to the interior of a large crystal, and difficulty dissipating stress from the deformation of the crystal structure. The size difference between the nano- and microcrystals is likely largely responsible for the different conversion ratios and this effect could be utilized to tune the amount of calcite conversion with respect to the SANCs. This selective partial conversion of the entire nanocomposite shows that while a unified material surface can be created with ion exchange reactions, material or size differences in building blocks can also be exploited for selective conversion.

## CONCLUSION AND OUTLOOK

In this paper, we show the potential of self-assembled nanocrystals (SANCs) to spatially direct and crystallographically orient the growth of microcrystals using an epitaxial match. Moreover, we demonstrate that the growth behavior of the microcrystals can be adjusted independently of the SANCs, making it possible to apply common strategies used for crystal growth manipulation. The nucleation and growth conditions of the microcrystals are nontrivial but can be tuned to form single

crystals on top of each nanocomposite structure. Additionally, we find that ion exchange reactions can be employed to transform the chemical surface of both nano- and microcrystals into a single material, enabling the formation of desired shapes from multiple components and materials without being constrained by the preferred geometries of the final desired material. Moreover, the ion exchange method allows to create combinations of microcrystals with materials they would not grow onto. These results highlight that SANCs can be leveraged as a highly versatile tool to direct crystal nucleation, thereby addressing key challenges in hierarchical material design.

The sequential approach to self-organization has many similarities to traditional organic chemistry in which complex molecules are routinely created from simple precursor molecules using sequential reactions. Inspired by the retrosynthesis approach in chemistry, we can break down a complex target structure into achievable building blocks and combine them using sequential self-organization. From this perspective, SANCs are a way to direct the nucleation of new materials in such subsequent steps, analogous to the functional groups of a molecule determining where the reaction takes place. Moreover, we already have indications that SANCs may be used for polymorph selection of materials, as their epitaxial match can be specific to only certain crystal structures.

Our study demonstrates how SANCs control nucleation through surface chemistry and epitaxial matching. We see this as a starting point for expanding nucleation strategies to accommodate a broader range of material systems and envision the development of a library with diverse nucleation directors to facilitate sequential self-organization. Another type of nucleation director could, for example, guide light to specific locations and initiate local photochemical reactions by utilizing

the shape of a waveguiding material or local plasmonic effects. Those photochemical reactions could induce the precipitation of a new material or even selectively dissolve the present material to then, as we have observed here, recombine with different ions and precipitate as a new material. We see the potential to develop diverse spatial nucleation directors beyond the type demonstrated in this article, allowing the expansion of material combinations beyond epitaxial matches for controlled sequential self-organization.

To unlock the full potential of sequential self-organization, we foresee the need to develop even more strategies analogous to those established in chemistry. For example, it is worth exploring which types of organization steps do not interfere with one another, similar to orthogonal reactions in chemistry. Some research on orthogonal conversion reactions specifically has already been conducted to integrate different chemical compositions.<sup>10</sup> For interfering reaction step combinations, strategies akin to protecting groups in synthetic chemistry should be developed. Such protection groups could be temporary coatings or even entire crystals to be removed after the step interfering with the integrity of the protected part of the structure. In our work, the silica matrix, in which the SANCs are embedded, could be cross-linked to function as a protective layer, for example. Moreover, separation and purification of chemical products are common practices in organic chemistry, while in self-organization, the focus often is on creating results as uniform as possible. A wider use of separation techniques for self-organized structures could broaden their applicability without sacrificing complexity for a uniform result. Overall, we see that while the length scales are fundamentally different, the molecular-scale principles of organic chemistry can serve as a great source of inspiration for the development of sequential self-organization strategies at the nano- and microscales. By combining these strategies with the control demonstrated in this study, sequential self-organization can be further advanced to enable increasingly complex and multifunctional materials.

## MATERIALS AND METHODS

**Materials.** All chemicals were used as purchased. Barium chloride dihydrate (ACS reagent,  $\geq 99\%$ ), calcium chloride dihydrate, sodium metasilicate, and ammonium carbonate (ACS reagent,  $\geq 30.0\%$   $\text{NH}_3$  basis) were purchased from Sigma-Aldrich. Manganese(II) chloride (for the synthesis) was purchased from Merck. All reactions were performed in deionized water ( $7 \mu\text{S}/\text{cm}$ ) previously purged with  $\text{N}_2$  for at least 2 h before use. The structures were grown on aluminum (0.3 mm thickness, 99% purity, GoodFellow) sample slides.

**Structure Growth.** The  $\text{BaCO}_3/\text{SiO}_2$  nanocomposites were grown on aluminum substrates in 15 mL of an aqueous degassed solution containing  $\text{BaCl}_2$  (20.2 mM) and  $\text{Na}_2\text{SiO}_3$  (8.65 mM). The substrates were positioned vertically in the fully prepared reaction solution. The reaction beaker was covered with a Petri dish to limit atmospheric  $\text{CO}_2$  influx through the spout. This basic setup is the same for all reactions, unless noted otherwise. The reactions were terminated after 1 h by removing the sample slides from the reaction solution. Subsequently, the slides were washed with water and acetone. This washing step was performed again after all individual growth steps.

In order to grow a  $\text{BaCO}_3$  microcrystal onto the nanocomposite, the substrate was reimmersed into an aqueous solution in such a way that the meniscus line formed a cross with the previous one where the structures grew. Each line of this cross stems from one of the growth phases, and at the intersection, growth from both reaction solutions occurs. The aqueous solution contained  $\text{BaCl}_2$  (20.2 mM), and its pH was raised to 11 using 1 M NaOH. To grow  $\text{BaCO}_3$  with a different shape, silica (3.1 mM) was used as an additive during the growth.

Calcite microcrystals were grown on nanocomposites in a variety of ways. The 15 mL aqueous solution contained  $\text{CaCl}_2$  (2.3–20.4 mM), and the carbonate formation was initiated either by raising the pH using NaOH (15  $\mu\text{L}$  0.01 M to 65  $\mu\text{L}$  1 M NaOH added) or by placing the reaction vessel in a desiccator equilibrated with ammonium carbonate salt. In order to grow single calcite crystals, 4.5 mM  $\text{CaCl}_2$  in the desiccator setup or a raised pH using 45–65  $\mu\text{L}$  1 M NaOH were found to be good parameters.

**Structure Conversion.** Created structures were converted right after they were grown to ensure that the silica was not cross-linked enough to hinder the reaction. For this, a substrate with fresh structures was placed in an air-sealed jar together with 650 mg of manganese(II) chloride, and the air was replaced with argon. Then, 50 mL of degassed and demineralized water was added to the jar. After 1 h, the substrate was removed and washed by dipping it into water and then acetone.

**Sample Analysis.** A Verios 460 SEM from FEI with an xT Microscope Control v5.5.2 build 3322 was used to take comparative images of the microarchitectures on the chosen sample slides by using 5 kV and 50 pA.

An X-MaxN 80 (Oxford Instruments) was used with 20 kV and 0.8 nA for the EDS analysis of characteristic structures to quantify their ion content and verify the conversion. The software AZtec 2.4 (Oxford Instruments) was used to interpret the collected EDS data. EDS map data of entire structures was acquired to determine the ion distribution of Ba, Ca, and Mn.

## ASSOCIATED CONTENT

### Supporting Information

The Supporting Information is available free of charge at <https://pubs.acs.org/doi/10.1021/acs.cgd.4c01450>.

Comparison of schematic illustrations with SEM images of crystal structures, SEM images of  $\text{BaCO}_3$  crystals grown in the presence of  $\text{SiO}_2$  as an additive, and EDS map sum spectra of structures in [Figure 5 \(PDF\)](#)

## AUTHOR INFORMATION

### Corresponding Authors

Joanna Aizenberg – Department of Chemistry and Chemical Biology, Harvard University, Cambridge, Massachusetts 02138, United States; John A. Paulson School of Engineering and Applied Sciences, Harvard University, Cambridge, Massachusetts 02138, United States; [orcid.org/0000-0002-2343-8705](https://orcid.org/0000-0002-2343-8705); Email: [jaiz@seas.harvard.edu](mailto:jaiz@seas.harvard.edu)

Willem L. Noorduyn – Van't Hoff Institute for Molecular Sciences (HIMS), Universiteit van Amsterdam, Amsterdam, XH 1098, The Netherlands; AMOLF, Amsterdam, XG 1098, The Netherlands; [orcid.org/0000-0003-0028-2354](https://orcid.org/0000-0003-0028-2354); Email: [w.noorduyn@amolf.nl](mailto:w.noorduyn@amolf.nl)

### Authors

Ariane V. Mader – Van't Hoff Institute for Molecular Sciences (HIMS), Universiteit van Amsterdam, Amsterdam, XH 1098, The Netherlands; AMOLF, Amsterdam, XG 1098, The Netherlands

René M. Williams – Van't Hoff Institute for Molecular Sciences (HIMS), Universiteit van Amsterdam, Amsterdam, XH 1098, The Netherlands; [orcid.org/0000-0002-9490-6182](https://orcid.org/0000-0002-9490-6182)

Complete contact information is available at: <https://pubs.acs.org/doi/10.1021/acs.cgd.4c01450>

### Author Contributions

A.V.M. contributed to conceptualization, methodology, investigation, data curation, writing—original draft, writing—review

and editing, and visualization. R.M.W. and J.A. contributed to writing—review and editing. W.L.N. contributed to conceptualization, methodology, investigation, writing—review and editing, and supervision.

## Notes

The authors declare no competing financial interest.

## ACKNOWLEDGMENTS

H. Schoenmaker is thanked for technical support. Scanning electron microscopy was performed at the fabrication and characterization facilities of the Amsterdam nanoCenter, supported by the NWO.

## REFERENCES

- (1) Espinosa, H. D.; Rim, J. E.; Barthelat, F.; Buehler, M. J. Merger of Structure and Material in Nacre and Bone - Perspectives on de Novo Biomimetic Materials. *Prog. Mater. Sci.* **2009**, *54*, 1059–1100.
- (2) Eder, M.; Amini, S.; Fratzl, P. Biological Composites—Complex Structures for Functional Diversity. *Science* **2018**, *362*, 543–547.
- (3) Hamm, C. E.; Merkel, R.; Springer, O.; Jurkojc, P.; Maiert, C.; Prechtelt, K.; Smetacek, V. Architecture and Material Properties of Diatom Shells Provide Effective Mechanical Protection. *Nature* **2003**, *421*, 841–843.
- (4) Weaver, J. C.; Milliron, G. W.; Miserez, A.; Evans-Lutterodt, K.; Herrera, S.; Gallana, I.; Mershon, W. J.; Swanson, B.; Zavattieri, P.; DiMasi, E.; et al. The Stomatopod Dactyl Club: A Formidable Damage-Tolerant Biological Hammer. *Science* **2012**, *336*, 1275–1280.
- (5) Grünewald, T. A.; Liebi, M.; Wittig, N. K.; Johannes, A.; Sikjaer, T.; Rejnmark, L.; Gao, Z.; Rosenthal, M.; Guizar-Sicairos, M.; Birkedal, H.; et al. Mapping the 3D Orientation of Nanocrystals and Nanostructures in Human Bone: Indications of Novel Structural Features. *Sci. Adv.* **2020**, *6*, 4171–4183.
- (6) Stifler, C. A.; Jakes, J. E.; North, J. D.; Green, D. R.; Weaver, J. C.; Gilbert, P. U. P. A. Crystal Misorientation Correlates with Hardness in Tooth Enamels. *Acta Biomater.* **2021**, *120*, 124–134.
- (7) Hendrikse, H. C.; Aguirre, A.; Van Der Weijden, A.; Meeussen, A. S.; D'Angelo, F. N.; Noorduin, W. L. Rational Design of Bioinspired Nanocomposites with Tunable Catalytic Activity. *Cryst. Growth Des.* **2021**, *21*, 4299–4304.
- (8) Helmbrecht, L.; Tan, M.; Röhrich, R.; Bistervels, M. H.; Kessels, B. O.; Koenderink, A. F.; Kahr, B.; Noorduin, W. L. Directed Emission from Self-Assembled Microhelices. *Adv. Funct. Mater.* **2020**, *30*, 1908218.
- (9) Noorduin, W. L.; Grinthal, A.; Mahadevan, L.; Aizenberg, J. Rationally Designed Complex, Hierarchical Microarchitectures. *Science* **2013**, *340*, 832–837.
- (10) Bistervels, M. H.; van der Weijden, A.; Schoenmaker, H.; Kamp, M.; Noorduin, W. L. Compose and Convert: Controlling Shape and Chemical Composition of Self-Organizing Nanocomposites. *Adv. Funct. Mater.* **2024**, *34*, 2403715.
- (11) Aizenberg, J.; Black, A. J.; Whitesides, G. M. Control of Crystal Nucleation by Patterned Self-Assembled Monolayers. *Nature* **1999**, *398*, 495–498.
- (12) Song, Q.; Yan, H.; Liu, K.; Xie, K.; Li, W.; Gai, W.; Chen, G.; Li, H.; Shen, C.; Fu, Q.; et al. Vertically Grown Edge-Rich Graphene Nanosheets for Spatial Control of Li Nucleation. *Adv. Energy Mater.* **2018**, *8*, 1800564.
- (13) Mishchenko, L.; Khan, M.; Aizenberg, J.; Hatton, B. D. Spatial Control of Condensation and Freezing on Superhydrophobic Surfaces with Hydrophilic Patches. *Adv. Funct. Mater.* **2013**, *23*, 4577–4584.
- (14) Li, L.; Fijneman, A. J.; Kaandorp, J. A.; Aizenberg, J.; Noorduin, W. L. Directed Nucleation and Growth by Balancing Local Supersaturation and Substrate/Nucleus Lattice Mismatch. *Proc. Nat. Acad. Sci. U. S. A.* **2018**, *115*, 3575–3580.
- (15) Carter, P. W.; Ward, M. D. Topographically Directed Nucleation of Organic Crystals on Molecular Single-Crystal Substrates. *J. Am. Chem. Soc.* **1993**, *115*, 11521–11535.
- (16) Mitchell, C. A.; Yu, L.; Ward, M. D. Selective Nucleation and Discovery of Organic Polymorphs through Epitaxy with Single Crystal Substrates. *J. Am. Chem. Soc.* **2001**, *123*, 10830–10839.
- (17) Hamilton, B. D.; Weissbuch, I.; Lahav, M.; Hillmyer, M. A.; Ward, M. D. Manipulating Crystal Orientation in Nanoscale Cylindrical Pores by Stereochemical Inhibition. *J. Am. Chem. Soc.* **2009**, *131*, 2588–2596.
- (18) Singh, A.; Lee, I. S.; Kim, K.; Myerson, A. S. Crystal Growth on Self-Assembled Monolayers. *CrystEngComm* **2011**, *13*, 24–32.
- (19) Han, Y.-J.; Aizenberg, J. Nucleation of Calcite Crystals Face-Selective Nucleation of Calcite on Self-Assembled Monolayers of Alkanethiols: Effect of the Parity of the Alkyl Chain. *Angew. Chem., Int. Ed.* **2003**, *42*, 3668–3670.
- (20) Ulman, A. Formation and Structure of Self-Assembled Monolayers. *Chem. Rev.* **1996**, *96*, 1533–1554.
- (21) Schreiber, F. Structure and Growth of Self-Assembling Monolayers. *Prog. Surf. Sci.* **2000**, *65*, 151–257.
- (22) Bragg, W. L. The Refractive Indices of Calcite and Aragonite. *Proc. R. Soc. London, Ser. A* **1924**, *105*, 370–386.
- (23) Speiser, D. I.; Eernisse, D. J.; Johnsen, S. A Chiton Uses Aragonite Lenses to Form Images. *Curr. Biol.* **2011**, *21*, 665–670.
- (24) Aizenberg, J.; Tkachenko, A.; Weiner, S.; Addadi, L.; Hendler, G. Calcitic Microlenses as Part of the Photoreceptor System in Brittlestars. *Nature* **2001**, *412*, 819–822.
- (25) Beniash, E.; Stifler, C. A.; Sun, C. Y.; Jung, G. S.; Qin, Z.; Buehler, M. J.; Gilbert, P. U. P. A. The Hidden Structure of Human Enamel. *Nat. Commun.* **2019**, *10*, 1–13.
- (26) Killian, C. E.; Metzler, R. A.; Gong, Y. U. T.; Olson, I. C.; Aizenberg, J.; Politi, Y.; Wilt, F. H.; Scholl, A.; Young, A.; Doran, A.; et al. Mechanism of Calcite Co-Orientation in the Sea Urchin Tooth. *J. Am. Chem. Soc.* **2009**, *131*, 18404–18409.
- (27) Seto, J.; Ma, Y.; Davis, S. A.; Meldrum, F.; Gourrier, A.; Kim, Y. Y.; Schilde, U.; Sztucki, M.; Burghammer, M.; Maltsev, S.; et al. Structure-Property Relationships of a Biological Mesocrystal in the Adult Sea Urchin Spine. *Proc. Nat. Acad. Sci. U. S. A.* **2012**, *109*, 3699–3704.
- (28) Li, L.; Weaver, J. C.; Ortiz, C. Hierarchical Structural Design for Fracture Resistance in the Shell of the Pteropod *Clio* Pyramidata. *Nat. Commun.* **2015**, *6*, 1–10.
- (29) Hyde, S. T.; Carnerup, A. M.; Larsson, A. K.; Christy, A. G.; García-Ruiz, J. M. Self-Assembly of Carbonate-Silica Colloids: Between Living and Non-Living Form. *Physica A* **2004**, *339*, 24–33.
- (30) García-Ruiz, J. M.; Melero-García, E.; Hyde, S. T. Morphogenesis of Self-Assembled Nanocrystalline Materials of Barium Carbonate and Silica. *Science* **2009**, *323*, 362–365.
- (31) Kaplan, C. N.; Noorduin, W. L.; Li, L.; Sadza, R.; Folkertsma, L.; Aizenberg, J.; Mahadevan, L. Controlled Growth and Form of Precipitating Microsculptures. *Science* **2017**, *355*, 1395–1399.
- (32) Nakouzi, E.; Rendina, R.; Palui, G.; Steinbock, O. Effect of Inorganic Additives on the Growth of Silica–Carbonate Biomorphs. *J. Cryst. Growth* **2016**, *452*, 166–171.
- (33) Kellermeier, M.; Glaab, F.; Carnerup, A. M.; Drechsler, M.; Gossler, B.; Hyde, S. T.; Kunz, W. Additive-Induced Morphological Tuning of Self-Assembled Silica–Barium Carbonate Crystal Aggregates. *J. Cryst. Growth* **2009**, *311*, 2530–2541.
- (34) Bistervels, M. H.; Kamp, M.; Schoenmaker, H.; Brouwer, A. M.; Noorduin, W. L. Light-Controlled Nucleation and Shaping of Self-Assembling Nanocomposites. *Adv. Mater.* **2022**, *34*, 2107843.
- (35) Bistervels, M. H.; Hoogendoorn, N. T.; Kamp, M.; Schoenmaker, H.; Brouwer, A. M.; Noorduin, W. L. Light-Controlled Morphological Development of Self-Organizing Bioinspired Nanocomposites. *Nanoscale* **2024**, *16*, 2310–2317.
- (36) Grimaldi, G.; Antony, L. S. D.; Helmbrecht, L.; Van Der Weijden, A.; Van Dongen, S. W.; Schuringa, I.; Borchert, J.; Alarcón-Lladó, E.; Noorduin, W. L.; Ehrler, B. Microstructuring of 2D Perovskites via Ion-Exchange Fabrication. *Appl. Phys. Lett.* **2021**, *119*, 223102.

(37) Van Der Weijden, A.; Van Hecke, M.; Noorduyn, W. L. Contraction and Expansion of Nanocomposites during Ion Exchange Reactions. *Cryst. Growth Des.* **2022**, *22*, 2289–2293.

(38) Hendrikse, H. C.; van der Weijden, A.; Ronda-Lloret, M.; Yang, T.; Bliem, R.; Shiju, N. R.; van Hecke, M.; Li, L.; Noorduyn, W. L. Shape-Preserving Chemical Conversion of Architected Nanocomposites. *Adv. Mater.* **2020**, *32*, 2003999.

(39) Opel, J.; Wimmer, F. P.; Kellermeier, M.; Cölfen, H. Functionalisation of Silica–Carbonate Biomorphs. *Nanoscale Horiz.* **2016**, *1*, 144–149.

(40) Opel, J.; Brunner, J.; Zimmermanns, R.; Steegmans, T.; Sturm, E.; Kellermeier, M.; Cölfen, H.; García-Ruiz, J. M. Symbiosis of Silica Biomorphs and Magnetite Mesocrystals. *Adv. Funct. Mater.* **2019**, *29*, 1902047.

(41) Bittarello, E.; Massaro, F. M.; Rubbo, M.; Costa, E.; Aquilano, D. Witherite (BaCO<sub>3</sub>)/ $\alpha$ -Quartz Epitaxial Nucleation and Growth: Experimental Findings and Theoretical Implications on Biomineralization. *Cryst. Growth Des.* **2009**, *9*, 971–977.

(42) Mader, A. V.; Helmbrecht, L.; Noorduyn, W. L. Multi-Layered Barium and Strontium Carbonate Structures Induced by the Small Organic Dye Acid Orange 7. *Cryst. Growth Des.* **2021**, *21*, 6349–6356.

(43) Bittarello, E.; Roberto Massaro, F.; Aquilano, D. The Epitaxial Role of Silica Groups in Promoting the Formation of Silica/Carbonate Biomorphs: A First Hypothesis. *J. Cryst. Growth* **2010**, *312*, 402–412.

(44) Addadi, L.; Moradian, J.; Shay, E.; Maroudas, N. G.; Weiner, S. A Chemical Model for the Cooperation of Sulfates and Carboxylates in Calcite Crystal Nucleation: Relevance to Biomineralization. *Proc. Nat. Acad. Sci.* **1987**, *84*, 2732–2736.

(45) Loste, E.; Park, R. J.; Warren, J.; Meldrum, F. C. Precipitation of Calcium Carbonate in Confinement. *Adv. Funct. Mater.* **2004**, *14*, 1211–1220.

(46) De Villiers, J. P. R. Crystal Structures of Aragonite, Strontianite, and Witherite. *Am. Mineral.* **1971**, *56*, 758–767.